Hidden dynamic allostery in a PDZ domain

Chad M. Petit[a], Jun Zhang[b], Paul J. Sapienza[a], Ernesto J. Fuentes[c], and Andrew L. Lee[a,b,1]

[a]Division of Medicinal Chemistry and Natural Products, Eshelman School of Pharmacy and [b]Department of Biochemistry and Biophysics, School of Medicine, University of North Carolina, Chapel Hill, NC 27599; and [c]Department of Biochemistry, University of Iowa, Iowa City, IA 52242

Edited by Susan S. Taylor, University of California San Diego, La Jolla, CA, and approved September 4, 2009 (received for review April 28, 2009)

Structure–function relationships in proteins are predicated on the spatial proximity of noncovalently interacting groups of atoms. Thus, structural elements located away from a protein's active site are typically presumed to serve a stabilizing or scaffolding role for the larger structure. Here we report a functional role for a distal structural element in a PDZ domain, even though it is not required to maintain PDZ structure. The third PDZ domain from PSD-95/SAP90 (PDZ3) has an unusual additional third alpha helix (α3) that packs in contiguous fashion against the globular domain. Although α3 lies outside the active site and does not make direct contact with C-terminal peptide ligand, removal of α3 reduces ligand affinity by 21-fold. Further investigation revealed that the difference in binding free energies between the full-length and truncated constructs is predominantly entropic in nature and that without α3, picosecond-nanosecond side-chain dynamics are enhanced throughout the domain, as determined by ^{2}H methyl NMR relaxation. Thus, the distal modulation of binding function appears to occur via a delocalized conformational entropy mechanism. Without removal of α3 and characterization of side-chain dynamics, this dynamic allostery would have gone unnoticed. Moreover, what appeared at first to be an artificial modification of PDZ3 has been corroborated by experimentally verified phosphorylation of α3, revealing a tangible biological mechanism for this novel regulatory scheme. This hidden dynamic allostery raises the possibility of as-yet unidentified or untapped allosteric regulation in this PDZ domain and is a very clear example of function arising from dynamics rather than from structure.

NMR | PSD-95 | spin relaxation | entropy

Proteins owe their functionality to the 3-dimensional arrangement of atoms. A typical protein's structure stabilizes its active site, allowing for specific interactions with substrate or ligand. These basic structure–function relationships are well understood for countless types of proteins. Because most active sites are relatively small, it has been presumed that the remaining bulk of the globular structure provides a scaffolding role. Thus, even though similar domains belonging to the same family may have substrate specificity preferences, the folds of those domains are composed of invariant structural elements (1). Nonetheless, variations in tertiary fold composition, such as additional elements of secondary structure, are not uncommon. An example of this can be seen within the PDZ domain family of proteins. From this, the question of whether there is a specific role for such auxiliary structural elements remains open. In other words, how might these additional elements influence the core domain?

PDZ domains (eg, PSD-95, Discs Large, Zo-1) are small, ≈90-aa modular structures that typically bind C-terminal tails (≈4–6 residues) of target proteins (2). They are frequently found in multiple copies in proteins with diverse functions, especially those involved in signal transduction complexes and in the anchoring of receptors at membrane specializations (2–4). Thus, one common function of PDZ domains is to provide scaffolding. Although the PDZ family has a highly conserved fold consisting of a 5- or 6-stranded half β-barrel and 2 α-helices (5), some members exhibit additional secondary structural elements or differences in lengths of helices, β-strands, or loops (6–9). For instance, the third PDZ domain from the PSD-95/SAP90 protein (referred to herein as PDZ3) contains an additional α-helix at its carboxyl terminus (α3) that was first reported in its homologue Dlg1 (5, 6). It is ironic that this atypical helix is present in PDZ3, because PDZ3 is considered the archetype of PDZ domains, being the first PDZ domain structure to be solved (2). Naively, α3 is not expected to impact function, because it lies on a different surface from the PDZ ligand-binding site (Fig. 1). However, studies on various proteins have shown that intramolecular communication can occur between sites that would not be expected to be energetically linked based on protein structure alone (10–14). This notion was exemplified early on in the PDZ domain family using coevolutionary analysis, from which an evolutionarily conserved communication pathway was proposed (15). Subsequently, individual PDZ domains were found to exhibit allosteric behavior (8, 16–19). For these reasons, we investigated the role of α3 in PDZ3 function, structure, and dynamics.

Here we show that the α3 appendage to PDZ3 modulates C-terminal peptide binding function through a novel, dynamics-based mechanism. Removal of α3 has a minimal effect on global PDZ3 structure, but results in a ≈21-fold reduction in binding affinity that is entirely entropic in origin, within experimental error. Backbone (^{15}N) and side-chain (^{2}H methyl) NMR relaxation experiments indicate that removal of α3 results in increased side-chain dynamics throughout the structure on time scales faster than ≈6 ns. These enhanced motions are quenched on peptide binding, providing the entropic driving force for the reduced binding affinity. This example of dynamically regulated binding combines features of dynamic allostery observed at the backbone level (20) with the control of ligand-binding affinity through the tuning of side-chain conformational entropy (21). These findings, along with the recent report that Tyr-397 in α3 is phosphorylated (22), provide support for the intriguing possibility that in vivo, PDZ3 function may be regulated by an entropically controlled dynamic mechanism. That this particular PDZ domain is not known to be allosteric or to undergo conformational change (5, 23) suggests that similar mechanisms might be found in other PDZ domains, such as PDZ from harmonin (24), or even in a wide variety of domain types.

Results

The third PDZ domain of the neuronal signaling protein PSD-95/SAP90 (PDZ3, residues 303–402) contains an uncharacteristic, third α-helix (α3, residues 394–399) at its C-terminus that packs up against the core domain (the widely conserved 5 or 6 β-strands and 2 α-helices) in a region distinct from the peptide ligand-binding pocket (Fig. 1) (5). The closest end-to-end approach between α3 and peptide is made at the −3 position (Gln) of peptide [using the numbering scheme of Doyle et al. (5)], whose side-chain nitrogen is located ≈6 Å from the hydroxyl oxygen of Tyr-397 (Fig. 1). There are no bridging waters, and the remaining residues of α3 and peptide ligand extend away from each other; all C^α–C^α distances are >10 Å. Thus, α3 does not directly contact the peptide. To investigate the role of α3 in PDZ3 function and behavior, a C-terminal truncation mutant (Δ7ct) was constructed with residues 396–402 removed. This

Author contributions: C.M.P. and A.L.L. designed research; C.M.P., J.Z., and E.J.F. performed research; C.M.P., J.Z., P.J.S., and E.J.F. analyzed data; and C.M.P. and A.L.L. wrote the paper.

The authors declare no conflict of interest.

This article is a PNAS Direct Submission.

[1]To whom correspondence should be addressed. E-mail: drewlee@unc.edu.

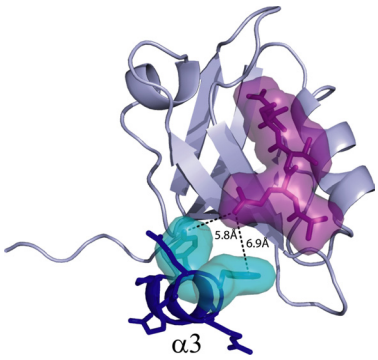

Fig. 1. Structure of PSD-95/SAP90 PDZ3 complexed with CRIPT peptide. The α3 helix is shown in blue. The van der Waals surface of the CRIPT peptide is in purple, and the nearest approaching residues (Tyr-397 and Phe-400) of α3 are in cyan.

truncation was engineered to disrupt the helix while leaving the core PDZ domain intact.

Consistent with previous studies (25), Δ7ct retains its native PDZ structure. The ^{1}H-^{15}N heteronuclear single quantum coherence (HSQC) spectrum shows a well-dispersed single set of peaks, indicative of a well-folded protein (Fig. 2). Aside from α3, all secondary structures are intact, as determined from $^{13}C^{\alpha}$ chemical shifts (26). A more detailed analysis of potential structural effects is provided below. These data show that Δ7ct is stable with a typical PDZ fold. Having verified no gross structural changes in Δ7ct, we set out to study the thermodynamics, structure, and dynamics of this system and found that α3 has a significant effect on both ligand-binding affinity and the internal dynamics of PDZ3.

Binding Thermodynamics of Δ7ct-PDZ3. Isothermal titration calorimetry (ITC) was used to evaluate the thermodynamic characteristics of Δ7ct and the full-length PDZ3 (i.e., PDZ3$^{303–402}$) binding to a peptide derived from the carboxyl terminus of CRIPT (Ac-TKNYKQTSV-COOH), a naturally occurring binding partner for PDZ3 (27). For PDZ3$^{303–402}$, binding occurs with relatively high affinity ($K_d = 1.2 \pm 0.1$ μM), whereas truncation lowers the affinity ($K_d = 25.7 \pm 3.6$ μM), as shown in Fig. 3 and summarized in Table 1. This demonstrates an important role for α3 in PDZ3's binding function. Interestingly, the enthalpic contribution to the free energy of binding is nearly identical for both constructs, whereas -TΔS changes from 1.7 kcal/mol for PDZ3$^{303–402}$ to 4.0 kcal/mol for Δ7ct at 25 °C (Table 1). Thus, the difference in binding is entropic in origin. Because binding takes place in a separate location from α3, and there is no change in the enthalpic contribution to binding

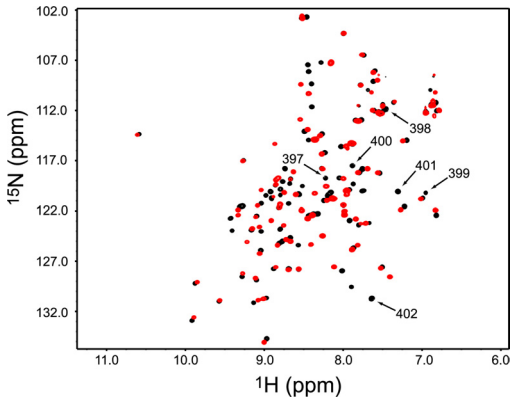

Fig. 2. ^{1}H-^{15}N HSQC spectrum of PDZ3$^{303–402}$ (black) overlain with the ^{1}H-^{15}N HSQC spectrum of Δ7ct (red). Resonances with ^{1}H-^{15}N assignments for deleted residues 396–402 are indicated by arrows.

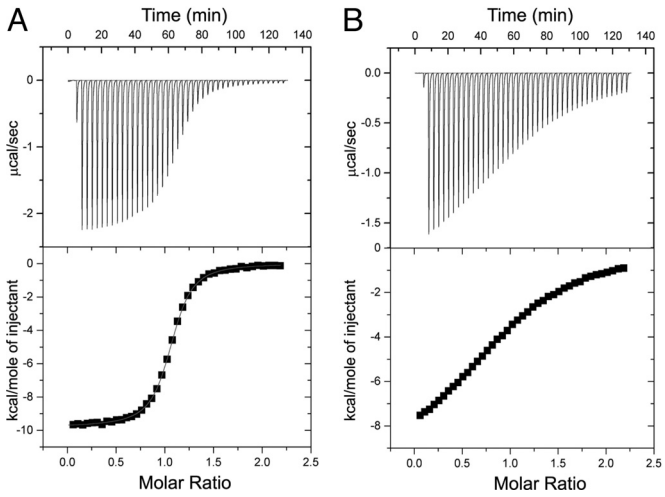

Fig. 3. The α3 helix affects CRIPT peptide binding. ITC data for binding of PSD-95/SAP90 PDZ3$^{303–402}$ (*A*) and Δ7ct (*B*) to C-terminal 9 residues of CRIPT (Ac-TKNYKQTSV-COOH) at 25 °C. Thermograms and integrated titration curves are shown in the top and bottom panels, respectively. Heats of dilution were obtained from independent buffer–buffer titration experiments (see *Materials and Methods*).

between the 2 constructs (which might reflect structural changes), differences in desolvation on binding are an unlikely source of the entropic change. It is possible that the core PDZ domain undergoes some structural adjustment such that individual changes in enthalpy cancel out, resulting in differences in desolvation on binding. There is no direct evidence of this, however. The remaining possible entropy-based explanation for the reduced affinity of Δ7ct for peptide is that significant changes in the conformational entropy of the system occur after removal of α3.

α3 Modulates Picosecond-Nanosecond Dynamics Throughout PDZ3. To investigate the source of any differences in conformational entropy on binding, we used backbone (28) and side-chain (29) NMR spin relaxation experiments to monitor the picosecond-nanosecond (ps-ns) dynamics of both the free and bound forms of PDZ3$^{303–402}$ and Δ7ct. For the backbone, ^{15}N T_1, T_2, and {^{1}H}-^{15}N NOE relaxation experiments were acquired at 2 field strengths (500 and 600 MHz) to achieve high-quality fits of the spectral density function. The relaxation analysis used statistical model selection to yield rigorous model-free order parameters for N-H bond vectors, S^2. The order parameter is a measure of a given bond's angular rigidity (on a scale of 0–1) on timescales faster than the overall rotational tumbling time (30), which in this case is on the order of 6 ns. For side-chain groups, methyl ^{2}H relaxation data sets (I_zC_z, $I_zC_zD_z$, and $I_zC_zD_y$) at 2 field strengths (500 and 600 MHz) were fitted to obtain the order parameter corresponding to the methyl C–CH_3 bond, denoted by S^2_{axis} (31).

Order parameters were first compared between PDZ3$^{303–402}$ and Δ7ct constructs in the absence of CRIPT peptide. Backbone N-H bond vectors showed limited changes in S^2 after removal of α3 (Fig. 4*A*). The largest observed changes were increased flexibility for a

Table 1. Thermodynamic parameters for the PDZ3–CRIPT peptide interaction at 25 °C

Protein	K_d (μM)	ΔH (kcal/mol)	−TΔS (kcal/mol)
PDZ3$^{303–402}$	1.2 (0.1)	−9.70 (0.12)	1.66 (0.06)
Δ7ct	25.7 (3.6)	−10.27 (0.68)	4.00 (0.59)

Values are the average of 2 independent experiments. The fitted stoichiometry (n) ranged from 0.95 to 1.06.

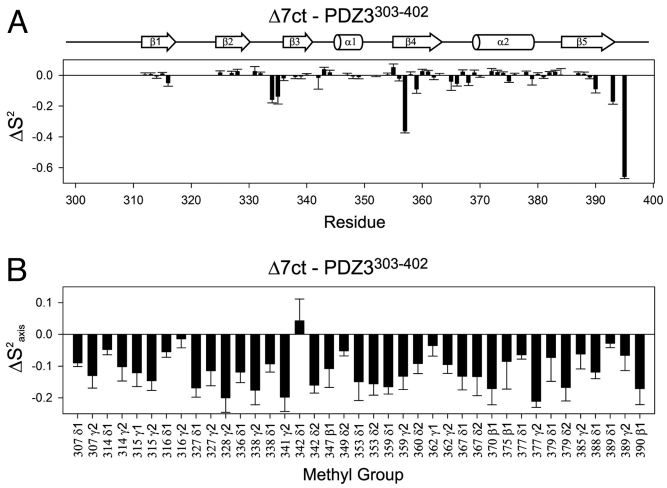

Fig. 4. α3 helix-dependent changes in backbone and side-chain order parameters. (*A*) Backbone HN groups (ΔS^2) as determined from ^{15}N relaxation. (*B*) Side-chain methyl groups (ΔS^2_{axis}) as determined from ^{2}H relaxation. S^2_{axis} values for PDZ3$^{303–402}$ were previously reported by Law et al. (44).

limited number of residues in the range of 0.1–0.4. Specifically, ΔS^2 values were −0.15 for residues Glu-334 and Gly-335 in the loop between β2 and β3, and −0.4 and −0.1, respectively, for residues Asp-357 and Ile-359 in β4. The changes also may reflect differences in the number of model-free parameters used (e.g., for 357, introduction of S^2_s in Δ7ct), which is a caveat of model selection. It also should be noted that no significant R_{ex} contributions (>2 Hz) were found in either of the 2 constructs. In addition, the carboxyl terminus of Δ7ct lacks an α3 structure and thus exhibited a large increase in flexibility relative to PDZ3$^{303–402}$. Otherwise, most of the backbone dynamics remained largely unaffected by the truncation, consistent with retention of global PDZ structure. In contrast, side-chain methyl groups showed significantly increased flexibility at most of the observed sites. Decreased S^2_{axis} values appear throughout the domain, with an average ΔS^2_{axis} (Δ7ct − PDZ3$^{303–402}$) of −0.12 and no apparent pattern (Fig. 4*B*).

In principle, a uniform decrease in S^2_{axis} values could be due to inaccurate determination of the global tumbling correlation time, τ_m, of either Δ7ct or PDZ3$^{303–402}$. Several lines of evidence strongly argue that this is not the case here. First, an inaccurate τ_m would lead to a uniform offset in backbone order parameters, which was not observed (Fig. 4*A*). Second, simulations showed that a relatively large error in τ_m (≈1 ns) would be needed to account for the majority of the observed decreases in S^2_{axis}. Global τ_m times of 5.9 ns and 6.0 ns were calculated for the PDZ3$^{303–402}$ and Δ7ct constructs, respectively, which are characteristic of a globular protein of ≈10 kDa (see *Materials and Methods* for all τ_m values). Third, both ^{15}N and ^{2}H relaxation on independent protein preparations of Δ7ct were performed, and measurements also were made on fresh Δ7ct samples of reduced concentration (0.3–0.4 mM). These data consistently yielded the same overall result, indicating increased side-chain flexibility in Δ7ct (data not shown). Finally, binding CRIPT peptide to Δ7ct resulted in S^2_{axis} values that were almost indistinguishable from the corresponding PDZ3$^{303–402}$ complex (see below). Thus, we conclude that the determined values of τ_m are accurate, and that the presence of α3 has a profound effect on the side-chain dynamics throughout the protein.

The ps-ns dynamics of Δ7ct and PDZ3$^{303–402}$ when bound to CRIPT peptide were also determined, completing the dynamics characterization of a cycle composed of peptide binding and presence or absence of α3 (Fig. 5). At the backbone level, overall changes in S^2 were negligible; the largest average S^2 change between any 2 forms was −0.02. At the side-chain level, as mentioned above, the average ΔS^2_{axis} ($\Delta 7ct_{free}$ − PDZ3$^{303–402}_{free}$) was found to be −0.12, indicating significant change in S^2_{axis}. The average ΔS^2_{axis} for the remaining sides of the cycle were determined to be 0.00 ($\Delta 7ct_{bound}$ − PDZ3$^{303–402}_{bound}$), 0.00 (PDZ3$^{303–402}_{bound}$ − PDZ3$^{303–402}_{free}$), and 0.12 ($\Delta 7ct_{bound}$ − $\Delta 7ct_{free}$). Unlike the backbone, many individual side-chain order parameters in both PDZ constructs are sensitive to peptide binding, similar to previous observations in another PDZ domain (16). It is worth reiterating that binding of peptide to Δ7ct caused extensive side-chain rigidification, such that the S^2_{axis} values of the complex were nearly indistinguishable from the PDZ3$^{303–402}$ complex (Fig. 5), with a Pearson correlation coefficient of 0.98. In simple terms, binding peptide to Δ7ct "snaps" the side-chain dynamics back to that of CRIPT-bound PDZ3$^{303–402}$.

In summary, removal of the α3 structural element in PDZ3 results in a significant global reduction in S^2_{axis}, indicating a global increase in side-chain flexibility for the truncation mutant, Δ7ct, relative to PDZ3$^{303–402}$. Binding peptide then returns the side-chain dynamics profile to that nearly identical with PDZ3$^{303–402}$. This global quenching of motions represents a substantial loss of conformational entropy and corroborates the calorimetrically observed entropic changes on binding.

Long-Range Modulation of Ligand Binding. Although α3-mediated enhanced peptide binding is entropy-driven, part of the binding affinity could be due to weak or transient interactions between α3 and the CRIPT peptide that are not visible in the crystal structure (5, 6). In that complex, no electron density was observed for the side chain of lysine at the −4 position or for any of the 4 preceding residues. To assess whether binding interactions might occur at other positions in the peptide, chemical shifts of the CRIPT peptide were monitored as a function of PDZ3 concentration from natural abundance ^{1}H-^{13}C HSQC spectra. The chemical shifts were assigned for free, unstructured peptide, and resonances were tracked in the presence of 7.5% and 15% molar ratios of PDZ3$^{303–402}$ to peptide. Normalized chemical shift changes (Δδ) were observed at positions 0 to −3, but no shift perturbations occurred at other, more N-terminal positions in the peptide (Fig. 6). This confirms that only the 4 C-terminal residues of the peptide ligand makes significant contact with PDZ3$^{303–402}$. More importantly, it rules out transient contacts between the Tyr at position −6 and elements of α3 that might explain how removal of α3 lowers binding affinity. We thus conclude that α3 is unequivocally distal to the CRIPT peptide-binding site and that α3 must confer binding energy through an indirect, allosteric mechanism.

Chemical shift perturbation analysis was used to assess how α3 affects PDZ structure as a function of peptide binding. Amide ^{15}N/^{1}H chemical shift changes (Δδ) in PDZ3$^{303–402}$ and Δ7ct in response to saturating amounts of CRIPT peptide were compared. Comparative shift perturbations due to peptide binding—rather than the raw effect of α3 removal—were used, because numerous shift perturbations in the PDZ core (Fig. 2) result from removal of the many interactions that α3 imparts, even without structural changes. Indeed, there are 4 aromatic side chains at this interface, 2 of which are on α3 (Tyr-397 and Phe-400). Removal of α3 thus leads to large changes in ring current shift effects in the PDZ core and in loop residues neighboring those aromatic groups. In contrast, comparative shift perturbations (in response to binding) subtracts out these α3 interface effects. Shift perturbations brought about by peptide binding in PDZ3$^{303–402}$ are closely mirrored in Δ7ct (Fig. 7). This indicates that α3 does not affect the structural response to peptide binding, which has been shown to be negligible for PDZ3$^{303–402}$ (5). Therefore, a structure-based mechanism for the long-range modulation of peptide-binding affinity is subtle at best and unlikely to be at work here, underscoring the importance of dynamics in this system.

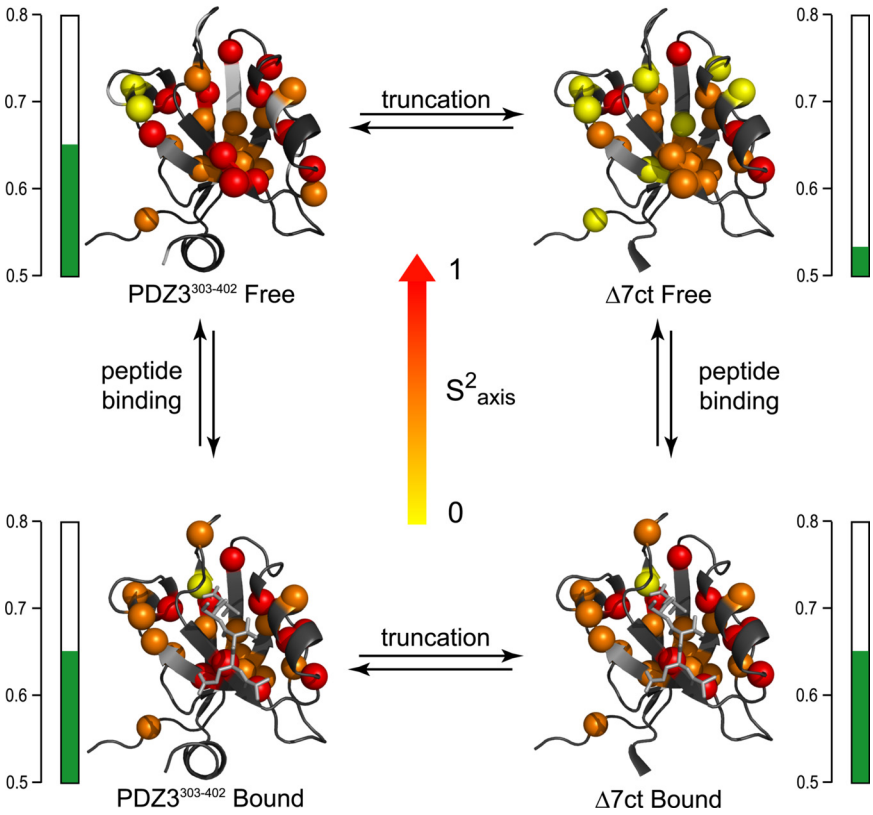

Fig. 5. Methyl side-chain dynamics of PDZ3$^{303-402}$ as a function of removal of α3 (left to right) and CRIPT peptide binding (top to bottom). C$^{\alpha}$ atoms of the corresponding methyl-bearing residues are color-coded according to S^2_{axis} parameters: yellow, $0 \leq S^2_{axis} \leq 0.4$; orange, $0.4 < S^2_{axis} < 0.7$; red, $0.7 \leq S^2_{axis} \leq 1$. Average S^2_{axis} values for each state are indicated by green bars.

Discussion

Here we report on a noncanonical structural appendage that regulates the internal dynamics and function of a common, conserved domain. Removal of the C-terminal third helix (α3) from the third PDZ domain (PDZ3$^{303-402}$) of PSD-95/SAP90 causes a global increase in ps-ns side-chain flexibility, which becomes quenched on the binding of C-terminal peptide ligand. This quenching incurs a conformational entropy penalty that is consistent with an overall reduction in CRIPT peptide affinity for the truncated construct (Δ7ct) relative to the longer PDZ3$^{303-402}$. Isothermal titration calorimetry confirmed that this reduction is entirely entropic in nature, within experimental error (Table 1). Because α3 is seated outside the ligand-binding pocket, differences in solvation do not easily explain this entropic effect. Therefore, given the direct observation of modulation in side-chain dynamics as detected by ^{2}H relaxation, the affinity reduction is explained by side-chain entropy, rather than by a structure-based mechanism. Thus, due to the (*i*) lack of signif-

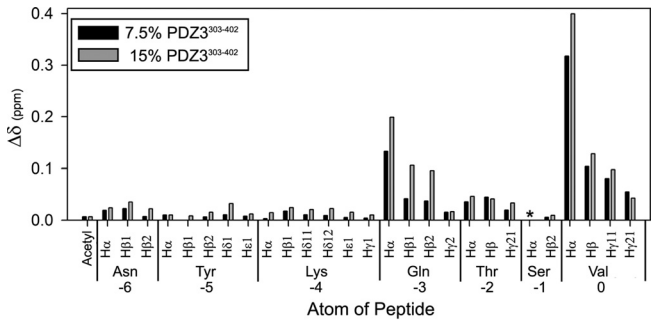

Fig. 6. Chemical shift perturbations in CRIPT 7-mer peptide (Ac-NYKQTSV-COOH) on addition of 7.5% and 15% molar ratios of PDZ3$^{303-402}$ to peptide. Shift perturbations were observed from natural abundance ^{1}H-^{13}C HSQC spectra. The asterisk denotes a lack of chemical shift data due to line broadening. Δδ is a weighted vector combination of ^{1}H and ^{13}C chemical shift perturbations, as described in *Materials and Methods*.

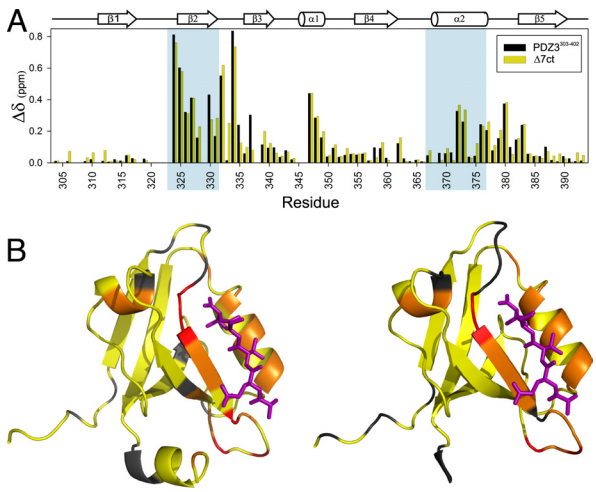

Fig. 7. Chemical shift perturbations of PDZ3 on peptide binding. (*A*) Combined ^{1}H and ^{15}N perturbations (defined in text) are shown for PDZ3$^{303-402}$ and Δ7ct constructs. Residues that make up the binding pocket are shaded in blue. (*B*) Chemical shift perturbations from (*A*) mapped onto the structure. Residues are color coded as follows: yellow, 0 ppm $\leq \Delta\delta \leq$ 0.2 ppm; orange, 0.2 ppm $< \Delta\delta <$ 0.5 ppm; red, 0.5 ppm $\leq \Delta\delta$.

icant structural changes, (*ii*) lack of direct interactions between α3 and CRIPT peptide residues, and (*iii*) participation of ps-ns side-chain dynamics throughout the domain, this α3/PDZ3/peptide ligand system is a clear example of allostery mediated by fast side-chain dynamics. It is allosteric in that α3 and the ligand are distal to one another, and it is also allosteric in the sense that it is driven by dynamic changes outside the ligand-binding site. We also note that several backbone sites, such as residues Glu-334 and Gly-335 in the glycine-rich β2-β3 loop, appear to behave like the side chains and contribute to the overall effect. Importantly, because this is observed in a small protein domain not prone to structural changes and considered "rigid" (23), it suggests that any folded protein could in principle use dynamic allostery as a regulatory mechanism, although recognition of this mechanism likely would require characterization of side-chain dynamics.

The finding that the distal α3 element can regulate PDZ3 function raises an interesting question as to whether this dynamic allostery has a defined biological role. In support of this, PSD-95 has been shown to be phosphorylated at multiple positions (32, 33), including Tyr-397 (22) located in the α3 helix. Because the Tyr phenol ring packs against the core PDZ domain, phosphorylation would alter α3 packing or lead to loss of α3 structure, either of which could affect ligand affinity. Although Tyr-397 is partially buried in the crystal structure, its accessibility to kinases should be significant, based on the high amide exchange rates within α3 (25) (data not shown for PDZ3$^{303-402}$). A particularly relevant finding comes from the *Drosophila* homologue Discs Large (Dlg) protein, which, along with PSD-95, belongs to the MAGUK (membrane-associated guanylate kinase) family of proteins (34). It was shown that deletion of a portion of α3 (residues corresponding to PSD-95 396–401) disrupts the interdomain communication between PDZ3 and the SH3-GK module located 25 residues downstream; in turn, this communication was shown to modulate Dlg binding to the localization protein GukHolder (35). This suggests that the highly conserved linker region between PDZ3 and the SH3 domains is essential for modulating both intramolecular and intermolecular interactions (35). Furthermore, it seems reasonable that the phosphorylation state and conformation of α3 could play an important role in this regulation. Thus, in a broader context, the dynamic allostery observed here with PDZ3 arises out of a larger, more complex interdomain regulatory scheme. Such regulatory modules within the context of larger interdomain interactions have previously been reported in the case of the GTPase exchange factor Vav1 (36).

Dynamics-based modulation of binding affinity has previously been reported in 2 notable cases. First, negative cooperative binding of cAMP to the dimeric catabolite activator protein was found to be driven by ps-ns backbone dynamics (20). Specifically, binding of the first cAMP occurs with little change in backbone flexibility, whereas binding the second cAMP triggers rigidification throughout both subunits and thus has a substantial conformational entropic cost (20). In the second example, changes in side-chain conformational entropy in calmodulin were shown to correlate remarkably well with calorimetric entropy changes for a series of calmodulin-binding peptides binding to calmodulin (21). In relation to these studies, the critical difference in the present study is that the long-range dynamic mechanism becomes apparent only after removal of the α3 helix. Furthermore, the driving force occurs through side-chain equilibrium dynamics, rather than effects from the backbone. In this sense, the data presented here bridge the side-chain entropy findings of Frederick et al. (21) with the dynamically driven allosteric effect reported by Popovych et al. (20). Our results provide further support for the general notion of entropy vis-à-vis dynamics as a bona fide mechanism for allosteric communication without conformational change (10, 37–39).

Materials and Methods

Cloning, Expression, and Purification of PSD-95/SAP90 PDZ3. The third PDZ domain of PSD-95/SAP90 from *Rattus norvegicus* was subcloned into a T7 expression vector (pET28a; Novagen) using primers designed to amplify residues 303–402 [using the numbering scheme of Doyle et al. (5)] of the full-length plasmid of PSD95/SAP90 (a gift from Ken Prehoda). The PSD-95 PDZ3 plasmid was transformed into DE3 Star *Eschericha coli* cells and grown in minimal media supplemented with the appropriate isotope for the desired labeling scheme, as described previously (16). A 50-mL starter culture was grown for 18 h and used to inoculate 950 mL of culture media. Protein expression was induced by adding isopropyl β-D-1-thiogalactopyranoside to a final concentration of 1 mM once the bacteria reached an OD_{600} of $\approx$0.6–0.8. The culture was allowed to grow for 4 h at 37 °C. Bacteria were harvested by centrifugation and frozen until further use. Frozen, pelleted cells were resuspended in lysis buffer [50 mM Tris, 150 mM NaCl, 10 mM EDTA (pH 6.8)] and lysed using 2 freeze–thaw steps followed by ultrasonication. The PDZ3$^{303-402}$ protein was purified using Source-Q (GE Biosciences) chromatography media, followed by Fast-Flow Q-Sepharose chromatography (GE Biosciences). Pooled fractions containing PDZ were subjected to size-exclusion chromatography using a G50-Sephadex column (GE Biosciences) equilibrated in NMR buffer [20 mM $NaPO_4$, 50 mM NaCl, 1 mM EDTA (pH 6.8)]. Typical yields were 30 mg/L with >95% purity, as verified by SDS/PAGE analysis.

Generation of Δ7ct. The Δ7ct truncation mutant (PSD-95/SAP90 numbering 303–395) was generated by PCR using oligonucleotides designed to amplify DNA within the α3 helix. This amplified DNA was subcloned into a T7 expression vector (pET28a; Novagen). Purification of truncated PDZ3 (Δ7ct) was achieved in the same manner as for PDZ3$^{303-402}$.

Peptide Synthesis. The C-terminal peptide from CRIPT (Ac-TKNYKQTSV-COOH or Ac-NYKQTSV-COOH) was manually synthesized using standard Fmoc solid-phase peptide chemistry. Peptide cleavage from the Wang resin and side-chain deprotection were achieved simultaneously using TFA:triisopropyl silane:anisole:water (90:5:3:2) for 2 h under nitrogen. The volume of filtrate was reduced under a stream of nitrogen, followed by peptide precipitation using 60 mL of cold diethyl ether. The mixture was extracted 3 times with 0.1% TFA in water (20 mL each). The aqueous phase was then combined and lyophilized. The crude powder was dissolved in water and then purified by reverse-phase (C18) HPLC using a linear gradient from 0 to 20% (95% acetonitrile, 4.9% water, 0.1% TFA) over 10 min, followed by a gradient from 20% to 35% over 15 min. Pure CRIPT was eluted at 20–22 min. The final peptide product was verified by mass spectrometry.

Isothermal Titration Calorimetry. ITC was carried out on a Microcal VP-ITC microcalorimeter at 25 °C. All measurements were collected by titration of CRIPT peptide into the protein solution. Both protein and peptide ITC buffer solutions were composed of 20 mM $NaPO_4$, 50 mM NaCl, and 1 mM EDTA (pH 6.8). The pH of the peptide and protein solutions were determined to be identical to within 0.02 pH units at room temperature. All solutions were degassed for $\approx$5–10 min without stirring and kept on ice before the ITC experiments.

For all ITC experiments, PDZ3 (100 μM) was placed in the sample chamber (ca. 2 mL), while the peptide solution (1 mM) was transferred into a 250-μL injection syringe. Each titration experiment comprised a single 2-μL injection, followed by 7-μL injections at 180-s intervals. The *c* values for PDZ3$^{303-402}$ and Δ7ct were $\approx$90 and $\approx$5, respectively. To account for the heat of dilution, an identical calorimetry experiment was performed in the absence of protein. The data from each experiment were collected and analyzed using ORIGIN version 5.0 (Microcal). Thermodynamic parameters were determined using nonlinear least squares fitting, assuming a single-site–binding model. The parameters reported are the results of 2 independent measurements.

NMR Spectroscopy. NMR experiments were carried out at 25 °C (calibrated using a methanol standard) using Varian Inova spectrometers equipped with $^{1}H/^{15}N/^{13}C$ probes and *z*-axis pulsed-field gradients operating at 500- and 600-MHz ^{1}H frequencies. For both PDZ3$^{303-402}$ and Δ7ct in free and bound forms, backbone and side-chain methyl groups were assigned using standard triple-resonance assignment experiments. Stereospecific assignments were obtained from a 10% ^{13}C-labeled PDZ3 sample (40). All NMR experiments were processed using NMRPipe and analyzed using NMRView compiled for Linux workstations (41, 42). Chemical shift perturbation analysis was performed using a weighted vector combination of shifts, calculated by applying the formulas $[\Delta\omega_H^2 + (0.25*\Delta\omega_C)^2]^{0.5}$ for ^{1}H-^{13}C shifts and $[\Delta\omega_H^2 + (0.1*\Delta\omega_N)^2]^{0.5}$ for ^{1}H-^{15}N shifts.

^{15}N Backbone Relaxation. ^{15}N T_1, T_2, and $\{^{1}H\}$-^{15}N NOE values were obtained through standard experiments (28) at 500 and 600 MHz for PDZ3$^{303-402}$ ($\approx$1.0 mM) and Δ7ct ($\approx$1.0 mM), both bound and free forms. For T_1 and T_2 experiments,

9 relaxation time points along with 3 duplicates were typically collected. For the {^{1}H}-^{15}N NOE, a recycle delay of 4.5 s was used. Relaxation decays were best fit to single exponentials using in-house programs. For Lipari-Szabo analysis, global τ_m correlation times were found to be 5.89 ns for PDZ3$^{303-402}_{free}$, 6.23 ns for PDZ3$^{303-402}_{bound}$, 5.98 ns for Δ7ct$_{free}$, and 6.34 ns for Δ7ct$_{bound}$. Anisotropic rotational models were tested, but it was concluded that the isotropic rotational model was the best for both PDZ3$^{303-402}$ and Δ7ct (data not shown). To assess potential aggregation effects on global τ_m, ^{15}N relaxation sets were independently collected and analyzed at 2 different concentrations (1.0 and 0.4 mM) for both constructs using independently prepared protein samples (data not shown). For each residue, the selection of 1 of 5 standard model-free models (S^2; S^2 and τ_e; S^2 and R_{ex}; S^2, τ_e, and R_{ex}; or S^2_s, S^2_f, and τ_s) were carried out using RVI software, a front-end interface for relxn2.2 that analyzes ^{15}N relaxation using simple model-free formalism (30) and the Akaike information criterion (43), as described previously (14).

^{2}H-Methyl Relaxation. Side-chain ^{2}H-methyl relaxation experiments were collected for samples containing randomly fractionally incorporated ^{2}H (29). Multicoherence relaxation experiments ($I_zC_zD_z$, $I_zC_zD_y$, and I_zC_z) were collected at 500 and 600 MHz (29). For each experiment, 9 relaxation time points along with 3 duplicate points were collected for PDZ3$^{303-402}$ ($\approx$1.0 mM) and Δ7ct ($\approx$1.0 mM) in both free and bound forms. All decays were best fit to single exponentials. Side-chain order parameters (S^2_{axis}) were derived from fits of S^2 and τ_e to the data using the appropriate isotropic τ_m values determined for each construct.

ACKNOWLEDGMENTS. We thank Karl Koshlap (UNC Eshelman School of Pharmacy, NMR Facility), Greg Young (UNC Biomolecular NMR Laboratory), Ashutosh Tripathy (UNC Macromolecular Interactions Facility), Dan Cline (UNC Eshelman School of Pharmacy), and Brenda Temple (UNC Structural Bioinformatics Facility) for their technical assistance. We also thank Ken Prehoda for providing DNA for the third PDZ domain of PSD-95. This work was funded by NSF grant 0344354 (to A.L.L.).

1. Bateman A, et al. (2002) The Pfam protein families database. *Nucleic Acids Res* 30:276–280.
2. Zhang MJ, Wang WN (2003) Organization of signaling complexes by PDZ-domain scaffold proteins. *Acc Chem Res* 36:530–538.
3. Garner CC, Nash J, Huganir RL (2000) PDZ domains in synapse assembly and signalling. *Trends Cell Biol* 10:274–280.
4. Kim E, Sheng M (2004) PDZ domain proteins of synapses. *Nat Rev Neurosci* 5:771–781.
5. Doyle DA, et al. (1996) Crystal structures of a complexed and peptide-free membrane protein-binding domain: Molecular basis of peptide recognition by PDZ. *Cell* 85:1067–1076.
6. Cabral JHM, et al. (1996) Crystal structure of a PDZ domain. *Nature* 382:649–652.
7. Birrane G, Chung J, Ladias JA (2003) Novel mode of ligand recognition by the Erbin PDZ domain. *J Biol Chem* 278:1399–1402.
8. Peterson FC, Penkert RR, Volkman BF, Prehoda KE (2004) Cdc42 regulates the Par-6 PDZ domain through an allosteric CRIB–PDZ transition. *Mol Cell* 13:665–676.
9. Mishra P, et al. (2007) Dynamic scaffolding in a G protein–coupled signaling system. *Cell* 131:80–92.
10. Pan H, Lee JC, Hilser VJ (2000) Binding sites in *Escherichia coli* dihydrofolate reductase communicate by modulating the conformational ensemble. *Proc Natl Acad Sci USA* 97:12020–12025.
11. Luque I, Leavitt SA, Freire E (2002) The linkage between protein folding and functional cooperativity: Two sides of the same coin? *Annu Rev Biophys Biomol Struct* 31:235–256.
12. Clarkson MW, Lee AL (2004) Long-range dynamic effects of point mutations propagate through side chains in the serine protease inhibitor eglin c. *Biochemistry* 43:12448–12458.
13. Gunasekaran K, Ma BY, Nussinov R (2004) Is allostery an intrinsic property of all dynamic proteins? *Proteins* 57:433–443.
14. Clarkson MW, Gilmore SA, Edgell MH, Lee AL (2006) Dynamic coupling and allosteric behavior in a nonallosteric protein. *Biochemistry* 45:7693–7699.
15. Lockless SW, Ranganathan R (1999) Evolutionarily conserved pathways of energetic connectivity in protein families. *Science* 286:295–299.
16. Fuentes EJ, Der CJ, Lee AL (2004) Ligand-dependent dynamics and intramolecular signaling in a PDZ domain. *J Mol Biol* 335:1105–1115.
17. Ota N, Agard DA (2005) Intramolecular signaling pathways revealed by modeling anisotropic thermal diffusion. *J Mol Biol* 351:345–354.
18. Gianni S, et al. (2006) Demonstration of long-range interactions in a PDZ domain by NMR, kinetics, and protein engineering. *Structure* 14:1801–1809.
19. van den Berk LC, et al. (2007) An allosteric intramolecular PDZ–PDZ interaction modulates PTP-BL PDZ2-binding specificity. *Biochemistry* 46:13629–13637.
20. Popovych N, Sun S, Ebright RH, Kalodimos CG (2006) Dynamically driven protein allostery. *Nat Struct Mol Biol* 13:831–838.
21. Frederick KK, Marlow MS, Valentine KG, Wand AJ (2007) Conformational entropy in molecular recognition by proteins. *Nature* 448:325–329.
22. Ballif BA, Carey GR, Sunyaev SR, Gygi SP (2008) Large-scale identification and evolution indexing of tyrosine phosphorylation sites from murine brain. *J Proteome Res* 7:311–318.
23. Chi CN, et al. (2008) Reassessing a sparse energetic network within a single protein domain. *Proc Natl Acad Sci USA* 105:4679–4684.
24. Pan L, Yan J, Wu L, Zhang M (2009) Assembling stable hair cell tip link complex via multidentate interactions between harmonin and cadherin 23. *Proc Natl Acad Sci USA* 106:5575–5580.
25. Feng H, Vu ND, Bai Y (2005) Detection of a hidden folding intermediate of the third domain of PDZ. *J Mol Biol* 346:345–353.
26. Wishart DS, Sykes BD (1994) The 13C chemical-shift index: A simple method for the identification of protein secondary structure using 13C chemical-shift data. *J Biomol NMR* 4:171–180.
27. Niethammer M, et al. (1998) CRIPT, a novel postsynaptic protein that binds to the third PDZ domain of PSD-95/SAP90. *Neuron* 20:693–707.
28. Farrow NA, et al. (1994) Backbone dynamics of a free and a phosphopeptide-complexed Src homology-2 domain studied by N-15 NMR relaxation. *Biochemistry* 33:5984–6003.
29. Muhandiram DR, Yamazaki T, Sykes BD, Kay LE (1995) Measurement of H-2 T-1 and T-1p relaxation times in uniformly C-13–labeled and fractionally H-2–labeled proteins in solution. *J Am Chem Soc* 117:11536–11544.
30. Lipari G, Szabo A (1982) Model-free approach to the interpretation of nuclear magnetic resonance relaxation in macromolecules, 1: Theory and range of validity. *J Am Chem Soc* 104:4546–4559.
31. Lipari G, Szabo A (1982) Model-free approach to the interpretation of nuclear magnetic-resonance relaxation in macromolecules, 2: Analysis of experimental results. *J Am Chem Soc* 104:4559–4570.
32. Morabito MA, Sheng M, Tsai LH (2004) Cyclin-dependent kinase 5 phosphorylates the N-terminal domain of the postsynaptic density protein PSD-95 in neurons. *J Neurosci* 24:865–876.
33. Du CP, et al. (2009) Increased tyrosine phosphorylation of PSD-95 by Src family kinases after brain ischaemia. *Biochem J* 417:277–285.
34. Fujita A, Kurachi Y (2000) SAP family proteins. *Biochem Biophys Res Commun* 269:1–6.
35. Qian Y, Prehoda KE (2006) Interdomain interactions in the tumor suppressor discs large regulate binding to the synaptic protein GukHolder. *J Biol Chem* 281:35757–35763.
36. Li P, Martins IR, Amarasinghe GK, Rosen MK (2008) Internal dynamics control activation and activity of the autoinhibited Vav DH domain. *Nat Struct Mol Biol* 15:613–618.
37. Cooper A, Dryden DTF (1984) Allostery without conformational change: A plausible model. *Eur Biophys J* 11:103–109.
38. Wand AJ (2001) Dynamic activation of protein function: A view emerging from NMR spectroscopy. *Nat Struct Biol* 8:926–931.
39. Tsai CJ, del Sol A, Nussinov R (2008) Allostery: Absence of a change in shape does not imply that allostery is not at play. *J Mol Biol* 378:1–11.
40. Neri D, et al. (1989) Stereospecific nuclear magnetic resonance assignments of the methyl groups of valine and leucine in the DNA-binding domain of the 434 repressor by biosynthetically directed fractional C-13 labeling. *Biochemistry* 28:7510–7516.
41. Johnson BA, Blevins RA (1994) NMR View: A computer program for the visualization and analysis of NMR data. *J Biomol NMR* 4:603–614.
42. Delaglio F, et al. (1995) NMRPIPE: A multidimensional spectral processing system based on Unix pipes. *J Biomol NMR* 6:277–293.
43. d'Auvergne EJ, Gooley PR (2003) The use of model selection in the model-free analysis of protein dynamics. *J Biomol NMR* 25:25–39.
44. Law AB, Fuentes EJ, Lee AL (2009) Conservation of side-chain dynamics within a protein family. *J Am Chem Soc* 131:6322–6323.